P. aeruginosa **disrupts ARP-2/3 mediated apical F-actin organization to induce intestinal deformation in** ***C. elegans***

Authors: AN Divyashree[1], Tanushree Sinha[1] and Anup Padmanabhan[1]*

Affiliations:

[1]Department of Biology, Trivedi School of Biosciences, Ashoka University, Sonipat, Haryana India -131029

*Correspondence to: anup.padmanabhan@ashoka.edu.in

ORCiD ids:

0000-0003-3127-2132 (AN Divyashree)

0009-0000-7405-283X (Tanushree Sinha)

0000-0001-6007-6929 (Anup Padmanabhan)

SUMMARY

Apico-basal polarity is crucial for maintaining cortical actin organization and regulating secretory functions in intestinal epithelium. The opportunistic pathogen, *Pseudomonas aeruginosa*, exploits the interplay between cell polarity and cytoskeletal machineries to subvert host defenses. Mechanistic insights into such pathogen-induced cytoskeletal alterations have largely been derived from *in-vitro* epithelial monolayers, which may not capture the influences of multicellular physiology such as tissue mechanics, and innate immunity. Here, we show that the extracellular *P. aeruginosa* disrupts apical polarity in *C. elegans* enterocytes, leading to fragmentation of ARP-2/3 clusters and disorganization of apical F-actin. This disruption causes shedding of actin-rich vesicles into lumen and a pronounced apical deformation. Inhibition of CDC-42-ARP-2/3-mediated actin polymerization or PI3K-AKT signalling attenuated enterocyte deformation and extended the lifespan of *C. elegans* upon *P. aeruginosa* exposure. Our findings reveal a conserved strategy by which *P. aeruginosa* exploits cellular polarity machinery to disrupt host actin organization during extracellular infection of the intestinal epithelium.

Keywords : actin cytoskeleton/ CDC-42 / cell polarity / *P. aeruginosa*/ Host-pathogen interactions

INTRODUCTION

Constantly exposed to a diverse micro-organisms, the intestinal epithelium acts as a frontline sentinel for immune surveillance, detecting perturbations caused by dysbiosis, distinguishing harmless commensals from pathogens, and mounting context-appropriate immune response. During infection, bacterial pathogens elicit a wide range of responses from intestinal epithelial cells - some orchestrated by the pathogens to promote their survival and dissemination, and others initiated by the host to limit damage and trigger innate immunity. Unlike professional immune cells, enterocytes lack canonical pathogen recognition receptors (PRRs) that detect microbe-associated molecular patterns (MAMPs). Instead, they respond to pathogen effector activity and the disruptions they cause to physiological processes and cellular homeostasis, collectively termed “patterns of pathogenesis”. These include damage associated molecular patterns (DAMPs) triggered by pathogen effectors. Studies in model organisms such as *Drosophila melanogaster* and *Caenorhabditis elegans (C. elegans)* have highlighted the role of effector-triggered, cell autonomous surveillance in epithelial tissue (Stuart *et al*, 2013; Tse-Kang *et al*, 2025; Vance *et al*, 2009).

C. elegans, a bacterivorous soil nematode, inhabits microbe-rich environments and encounters a broad spectrum of microorganisms, including pathogens (Berg *et al*, 2016; Schulenburg & Félix, 2017). While a protective cuticle (Gravato-Nobre *et al*, 2005) and sophisticated pathogen-avoidance behaviours (Lei *et al*, 2024; Melo & Ruvkun, 2012; Pereira *et al*, 2020; Prakash *et al*, 2021; Singh & Aballay, 2019b; Zhang *et al*, 2005) limits pathogen exposure, the intestinal epithelium remains the primary site of infection due to the worm’s bacterial diet. Ingested bacteria are mechanically ground in the pharynx before entering the lumen, yet some pathogens survive, proliferate, and colonize the intestine. The *C. elegans* intestine is composed of 20 polarized epithelial cells arranged longitudinally, with apical surfaces facing the central lumen and basolateral surface engaged in cell-cell and cell-matrix adhesions (Dimov & Maduro, 2019; McGhee, 2007). The apical surface is enriched in microvilli, providing the primary site for host-pathogen interaction (MacQueen *et al*, 2005a) (Fig. 1A). Polarity is maintained by structural and signalling complexes: the Crumbs complex (CRB-1, CRB-3, MAGUK-2) and the PAR complex (comprising PAR-3, PAR-6, PKC-3 kinase and CDC-42 GTPase) localize apically, while the Scribble complex (LET-

413, LGL-1, and DLG-1) and PAR-1 kinase localize basolaterally. Lipids are also polarized, with phosphatidylinositol 4,5-bisphosphate [PI(4,5)P_2 or PIP_2] enriched apically and phosphatidylinositol 3,4,5-trisphosphate [PI(3,4,5)P_3 or PIP_3] basolaterally. This polarity is reinforced by polarity complexes, cytoskeletal organization, membrane trafficking, and junctional assemblies. (Armenti & Nance, 2012; Bossinger *et al*, 2004; Legouis *et al*, 2000; Winter *et al*, 2012). Membrane polarity is also essential for the spatial localization and activation of Rho family GTPases (Jaffe & Hall, 2005). In particular, CDC-42 activates the ARP-2/3 complex to promote branched actin polymerization, essential for the assembly and maintenance of apical microvilli (Bernadskaya *et al*, 2011; Ma *et al*, 1998; Martin-Belmonte *et al*, 2007; Shafaq-Zadah *et al*, 2012; Thuenauer *et al*, 2022). During infection many pathogens employ diverse virulence strategies to subvert the host polarity and actin cytoskeletal machinery to alter cellular shape and mechanics (Ruch & Engel, 2017). This facilitates intracellular entry and spread, or extracellular effector-induced inflammation and tissue damage (Bastounis *et al*, 2022; Colonne *et al*, 2016). Conversely, epithelial cells may actively reorganize actin as part of their defense response. Thus, plasma membrane polarity-actin cytoskeleton cross talk is vital for epithelial integrity during infection (Fleiszig *et al*, 1997; Tran *et al*, 2014).

The opportunistic pathogen, *Pseudomonas aeruginosa* a major cause of nosocomial infections and infects a wide range of hosts, including *C. elegans* (Balla & Troemel, 2013; Mahajan-Miklos *et al*, 1999; Tan *et al*, 1999a). In worms, *P. aeruginosa* infection induces diverse stress responses, mitotic quiescence, and apoptosis (Kuss-Duerkop & Keestra-Gounder, 2020; Pellegrino *et al*, 2014; Dunbar *et al*, 2012; McEwan *et al*, 2012; Bollen *et al*, 2024). In the absence of professional immune cells, *C. elegans* upon detecting infection, activates innate immune signalling such as the TIR-1-p38 MAP kinase and the DAF-2/DAF-16 insulin/IGF-1 pathways (Peterson *et al*, 2023). DAF-2 dependent phosphorylation of PI3K/AGE-1 recruits AKT-1/AKT-2 kinases that in turn phosphorylate DAF-16. This kinase cascade results in cytoplasmic retention of DAF-16, thereby regulating gene expression (Ewbank, 2006). DAF-16 is known to induce expression of antimicrobial genes, detoxifying enzymes and bacterial avoidance (Balla & Troemel, 2013; Cohen & Troemel, 2015; Irazoqui *et al*, 2010; Peterson *et al*, 2022; Pukkila-Worley & Ausubel, 2012). Avoidance behaviour is also

triggered by mechanical cues, such as intestinal distension ("bloating"), mediated by TRPM channels (Filipowicz *et al*, 2021; Kumar *et al*, 2019; Singh & Aballay, 2019b, 2019a). Here, we investigated the mechanism underlying cytoskeletal remodelling and polarity disruption following *P. aeruginosa* infection. We find that *P. aeruginosa* exploits PI3K-AKT pathway to perturb CDC-42-ARP-2/3-mediated actin organization in *C. elegans* enterocytes. The resultant disruption in epithelial polarity and discharge of actin rich vesicles from the apical surface locally alters the surface mechanics resulting in a deformed intestinal lumen surface that is associated with decreased organism viability.

RESULTS

Pseudomonas aeruginosa infection results in *C. elegans* intestinal deformation

Consistent with previous studies, exposure to *P. aeruginosa* strain PA14 resulted in reduced *C. elegans* survival (TD_{50}^{PA14} ~3 days) compared to *E. coli* (OP50) (TD_{50}^{OP50} ~8 days) (Fig. 1B). This lethality has been partly attributed to the colonization of the intestinal lumen by *P. aeruginosa* (Tan *et al*, 1999a). To examine the impact of *P. aeruginosa* infection on host cytoskeletal organization, we imaged *C. elegans* intestines expressing mCherry fused to the N-terminus of ACT-5, the intestine-specific actin isoform (MacQueen *et al*, 2005b; Szumowski *et al*, 2016). In *E. coli*-fed worms, ACT-5 appeared as a smooth parallel lining along the intestinal lumen (Fig. 1B and 1C; blue arrowhead, OP50). Despite age related intestinal distension (Egge *et al*, 2019; Irazoqui *et al*, 2010; Singh & Aballay, 2019a), the ACT-5 signal remained smooth even after 3 days on *E. coli* (Fig.1C; red double-headed arrows in OP50/day-3, and S1A). Although lumen was distended following *P. aeruginosa* exposure (Fig. 1C, red double-headed arrows in PA14 day-3, and Fig S1A), apical surface characteristics were markedly distinct. In contrast to the smooth surface seen in *E. coli*-fed animals, *P. aeruginosa*-fed worms displayed extensive wrinkles and surface deformations (Fig. 1C; PA14,filled red arrowheads), with vesicle-like structures budding outward from the deformed apical surface (Fig. 1C; PA14, red arrows in enlarged ROI). Compared to only ~4% (2/54) of *E. coli*-fed worms, ~48%(27/56) of *P. aeruginosa*-exposed worms showed such deformations after 1-day (Fig. 1C). By day-3, the incidence rose to ~83% (43/52) in *P. aeruginosa*-fed worms compared to ~19% (10/52) on *E. coli* (Fig. 1D).

Magnitude of intestinal deformation depends on the duration *of P. aeruginosa* infection

To quantify changes in intestinal morphology, we defined a dimensionless "apical deformation index" (δ_{apical}), as the ratio of apical lumen length to total worm length (Fig. 1E). *E. coli*-fed worms consistently maintained '$\delta_{apical}^{OP50}=1$', whereas *P. aeruginosa* exposure resulted in '$\delta_{apical}^{PA14}>1$', with values increasing over time, indicating

149 progressive deformation (Fig. 1F). Tracking individual worms revealed that those fed
150 with *E. coli* , the value of δ_{apical}^{OP50} remained ~1, but in worms exposed to *P.*
151 *aeruginosa*, deformation was evident by day-1 and worsened over subsequent days
152 (Fig. 1G). In acute infection assays, 12-hour exposure did not cause significant
153 deformation, whereas 24-hour exposure induced noticeable apical distortion even
154 after transfer back to *E.coli* (Fig. S1B). To test whether deformation extended beyond
155 the apical surface, we examined transgenic worms co-expressing LET-413::mCherry
156 and DLG-1::GFP, the Scribble and Discs Large orthologs in *C. elegans,* as markers
157 for basolateral surface and adherens junctions (AJ), respectively (Bossinger *et al*,
158 2004; Legouis *et al*, 2000; McMahon *et al*, 2001; Riga *et al*, 2021). Neither AJ
159 positioning nor basal deformation index (δ_{basal}) was significantly altered by *P.*
160 *aeruginosa* exposure (Fig. 5A and S1C). However, lateral surfaces showed LET-413
161 enrichment and altered morphology (Fig. 5A and 5C), indicating that deformation was
162 restricted to apical and lateral domains.

163 Next we confirmed that the intestinal deformation was independent of oocytes or
164 uterine expansion following fertilization by examining males (Fig. S1D and S1E). F-
165 actin staining using Phalloidin-AlexaFluor647 and LifeACT::mRuby expression
166 showed visible apical deformation specifically upon *P. aeruginosa* exposure,
167 eliminating the possibility that the infection phenotype might be an artifact of
168 mCherry::ACT-5 transgene expression (Fig. S1F and S1H, red filled arrowheads).
169 Finally, we validated the phenotype using additional apical/sub-apical markers: PGP-
170 1::GFP, ERM-1::GFP, PAR-6::GFP, and IFB-2::GFP, that localized to apical
171 membrane, microvillar structure or subapical positions, respectively (Fig. 1H) (Geisler
172 *et al*, 2020; Göbel *et al*, 2004; Sepers *et al*, 2022). In all cases, *P. aeruginosa* exposure
173 resulted in clear deformation of the apical surface topology.

174 'Slow killing' assay, typically uses nematode growth media (NGM) containing 0.35%
175 peptone (Tan *et al*, 1999a). To minimize any confounding effects from elevated
176 peptone concentrations on intestinal epithelial response, we conducted our infections
177 on standard NGM containing 0.25% peptone, optimised for *C. elegans* growth
178 (Stiernagle, 2006). We observed intestinal deformation in worms infected on 0.35%
179 peptone media indistinguishable from 0.25% peptone (Fig. S1I and S1J). Our lifespan
180 assays mirrored previously reported kinetics using 0.35% peptone-containing NGM

181 (Figure 1A) (Tan *et al*, 1999a). Thus we confirmed that our infection conditions
182 faithfully recapitulate chronic *P. aeruginosa* infection, leading to progressive apical and
183 lateral intestinal deformation.

184

185 **CDC-42 mediates *Pseudomonas*-induced intestinal deformation**

186 Members of RHO family GTPases, primarily RHO-1, RAC-1, and CDC-42, are key
187 upstream regulators of F-actin assembly and organization, that co-ordinate actin
188 dynamics in a spatiotemporally controlled manner (Ann Mack & Georgiou, 2014; Jaffe
189 & Hall, 2005). *P. aeruginosa* -infecting MDCK cells disrupt RHO signalling through
190 effector proteins that interfere with GTPase-activating proteins (GAPs), leading to the
191 disorganization of actin architecture (Cowell *et al*, 2005; Kazmierczak & Engel, 2002;
192 Krall *et al*, 2000; Pederson *et al*, 1999; Sun & Barbieri, 2004). To test whether *P.*
193 *aeruginosa*-induced surface deformation in *C. elegans* enterocytes might similarly
194 depend on RHO GTPase-mediated actin re-organization, we individually depleted
195 RHO-1, CED-10 (RAC-1), and CDC-42 in adult worms expressing intestinal
196 mCherry::ACT-5, and subsequently exposed them to *P. aeruginosa* or *E. coli*. As in
197 the RNAi control, exposure to *P. aeruginosa* resulted in apical deformation in *rho-*
198 *1(RNAi)* or *ced-10(RNAi)* animals (Fig. 2A, S2A and S2B). In contrast, *cdc-42(RNAi)*
199 worms exposed to *P. aeruginosa* displayed no deformation (Fig. 2A and 2B). This lack
200 of deformation was not due to impaired pathogen sensing in *cdc-42(RNAi)* worms (Fig.
201 S2D and S2E) (Estes *et al*, 2010). Consistent with its role in suppressing intestinal
202 deformation, *cdc-42(RNAi)* worms exhibited significantly extended lifespan (8 days)
203 compared to RNAi controls (4 days) upon *P. aeruginosa* exposure (Fig. 2C).

204

205 ***P. aeruginosa* infection leads to cytoplasmic accumulation of G-actin**

206 The absence of intestinal deformation in *cdc-42(RNAi)* worms prompted us to
207 investigate the intracellular localization of CDC-42 and its downstream effector, the
208 actin nucleating ARP-2/3 complex, during *P. aeruginosa* infection. We used worms co-
209 expressing ARX-2::TagRFP (an essential subunit of the ARP-2/3 complex) at its
210 endogenous locus, and CDC-42::GFP, expressed exogenously under the native *cdc-*

211 *42* promoter (Neukomm *et al*, 2014; Wu *et al*, 2017). In control animals maintained on
212 *E. coli*, both CDC-42 and ARX-2 localized predominantly to the apical membrane of
213 the enterocytes, with little accumulation in the cytoplasm over 2 days of exposure (Fig.
214 2D and 2G; OP50 panel and Fig. S2C). Upon exposure to *P. aeruginosa*, both
215 cytoplasmic and apical CDC-42 levels increased markedly (Fig. 2D enlarged ROI, 2E
216 and 2F). Cytoplasmic levels of ARX-2 also increased (~2.6 fold) (Fig. 2H) though
217 apical ARX-2 remained unchanged relative to *E. coli* (Fig. 2I). Intracellular actin
218 mirrored that of ARX-2, with ~2.5 fold increase in cytoplasmic levels but none in apical
219 levels (Fig. 2J- 2L). Surprisingly, Phalloidin-AlexaFluor647 staining and
220 LifeACT::mRuby did not show any cytoplasmic staining, suggesting that the
221 accumulated cytoplasmic actin pool is primarily G-actin (Fig. S1F-S1H). Thus, the
222 increased cytoplasmic levels following *P. aeruginosa* infection reflects accumulation
223 of G-actin rather than loss of F-actin from the apical surface.

224

225 **_P. aeruginosa_-induced disruption of cortical actin results in apical surface**
226 **deformation**

227 It seemed counterintuitive that apical ARX-2 and ACT-5 intensities did not increase
228 despite CDC-42 enrichment. To clarify this conundrum, we measured apical levels of
229 ACT-5 and ARX-2 in *cdc-42(RNAi)* worms, and found them to be significantly reduced
230 (see OP50 panels in Figs. 3A, S3A, S3B and S3D). Thus apical actin and ARP-2/3
231 complex are sensitive to CDC-42-depletion, but not to *P. aeruginosa*-induced CDC-
232 42-enrichment. The absence of deformation in *cdc-42(RNAi)* animals could therefore
233 reflect a direct effect of CDC-42 depletion or an indirect effect via reduced ARP-2/3-
234 mediated F-actin polymerization. To distinguish these, we depleted ACT-5 or ARX-2
235 in worms co-expressing CDC-42::GFP and ARX-2::TagRFP. Due to *act-5(RNAi)*-
236 associated developmental defects, analyses were restricted to day 1 post-infection.
237 Strikingly, *act-5(RNAi)* and *arx-2(RNAi)* worms, like *cdc-42(RNAi)* showed rescue of
238 deformation phenotype following infection despite elevated CDC-42 levels (red open
239 arrowheads in Fig.3C-E,3G and S3E).

240 To probe the function of ARP-2/3 dependent actin polymerization in *P. aeruginosa*-
241 induced intestinal deformation, we analysed worms co-expressing mCherry::ACT5

242 and an apical membrane maker, PGP-1::GFP. In control worms fed with *E. coli*, ACT-
243 5 and PGP-1 were uniformly co-localized at the apical surface (Fig. 3F; control panel).
244 In *arx-2(RNAi)* intestines, apical actin was absent and instead appeared as
245 cytoplasmic aggregates, even when fed with *E. coli* (Fig. 3F; *arx-2(RNAi)* red filled
246 arrowheads). This ruled out cytoplasmic actin accumulation as a possible cause of *P.*
247 *aeruginosa*-induced deformation. ARP-2/3 disruption has been implicated in
248 cytoplasmic mislocalization of membrane bound components such as DLG-1 and
249 ERM-1 (Bernadskaya *et al*, 2011). PGP-1 displayed diffused apical localization in *arx-*
250 *2(RNAi)* intestines (Fig. 3F; *arx-2(RNAi)* red hollow arrowheads). These results
251 suggested the central role of ARP-2/3 polymerized actin in maintenance of apical
252 membrane organization. Importantly, CDC-42 and ARX-2 maintained apical
253 localization even in the absence of actin (Fig. 3F and 3G), confirming their upstream
254 role in the actin polymerization pathway. Collectively, these results demonstrate that
255 rescue of apical deformation in *cdc-42(RNAi)* and *arx-2(RNAi)* intestines following *P.*
256 *aeruginosa* exposure was due to disruption of ARP-2/3 mediated actin polymerization.

257

258 **Fragmented ARP-2/3 clustering and F-actin disorganization drive release of**
259 **membrane vesicles into the intestinal lumen following *P. aeruginosa* exposure.**

260 Although overall intensities of apical ARX-2 and ACT-5 were comparable between
261 worms exposed to *P. aeruginosa* and *E. coli* (Fig. 2I and 2L), their surface localization
262 patterns were markedly distinct. In *E. coli*-fed worms, ARX-2 was evenly distributed at
263 the apical surface (Fig. 4A; OP50, cyan arrowhead) essential for contiguous actin
264 polymerization, supporting brush border integrity (Bidaud-Meynard *et al*, 2021;
265 MacQueen *et al*, 2005b; Stutz *et al*, 2015). In contrast, *P. aeruginosa*-infected animals
266 exhibited fragmented ARX-2 clusters, interspersed with ARX-2-depleted regions (Fig.
267 4A; PA14, white arrows). We sought to correlate the cortical actin distribution with this
268 fragmented ARP-2/3 localization using worms co-expressing mCherry::ACT-5 and
269 ARX-2::GFP. Medial confocal sections of intestines from this strain when exposed to
270 *P. aeruginosa* resulted in apical actin to protrude as a 'bud-like' structure into the
271 lumen, emerging from ARX-2-free apical surface (Fig 4B; actin protrusions - yellow
272 arrowheads, fragmented ARP-2/3 – cyan arrows and Fig. 1C; red arrows in enlarged
273 ROI). By day-2, these protrusions pinched off as vesicles, coinciding with apical

surface deformation (Fig. 1C; day-2 PA14 panel - red arrows in enlarged ROI and Fig. 4D -cyan arrows in enlarged ROI). Lattice light sheet microscopy of the intestinal lumen surface of animals expressing mCherry::ACT-5 exposed to *P. aeruginosa* expressing GFP revealed extracellular pinching of actin rich vesicles from the apical surface into the lumen (Fig. 4C; enlarged ROI, cyan arrows).

To determine whether these extracellular actin structures were membrane-enclosed, we examined worms co-expressing mCherry::ACT-5 and PGP-1::GFP. Medial confocal images on day-2 post-infection revealed apical buds at various stages: initial protrusion (Fig. 4D; ROIs 1a & 2a), membrane pinching (1b & 2b), and free vesicles in the lumen (cyan arrows, 1c & 2c). Intensity line-scan analysis confirmed that these vesicles consisted of cortical actin cores surrounded by PGP-1::GFP-labelled apical membrane. LifeACT::mRuby labeled these vesicles, indicating filamentous actin content (Fig. 4E). We estimated the vesicle diameter to be ~ 0.59 μm (Fig. S4A). These results support the view that *P. aeruginosa* exposure led to disordered ARP-2/3 localization at the apical lumen surface destabilising cortical actin organization, resulting in the release of F-actin rich vesicles from the apical surface into lumen.

P. aeruginosa **infection disrupts apical polarity of enterocyte epithelium**

Fragmented ARP-2/3 clustering and vesicle shedding suggested a loss of apical membrane identity. *P. aeruginosa* attachment to MDCK cells triggers a transient PI(3,4,5)P_3 accumulation at the apical surface, resulting in the loss of apical membrane identity (Kierbel *et al*, 2007, 2005; Thuenauer *et al*, 2022). To check if *P. aeruginosa* might cause a similar disruption to the polarity in *C. elegans* intestinal epithelium, we analysed the localization of the *C. elegans* Scribble homolog, LET-413 and the cell junction marker, DLG-1. The LET-413 complex and DLG-1 have been reported to be essential for maintenance of basolateral domains in *C. elegans* by regulating the localization of apical polarity components (Bossinger *et al*, 2004; McMahon *et al*, 2001). In *E. coli*-fed worms, the localization of LET-413 was limited to the basolateral membrane with the apical surface largely devoid of any LET-413 (Fig. 5A; OP50 panel, basolateral surface -yellow filled arrowhead, apical surface -yellow asterisks) (Legouis *et al*, 2000). Upon exposure to *P. aeruginosa,* we observed a

305 significant increase in LET-413 levels along the apical and lateral membranes (Fig.
306 5A; PA14 panel, apical surface - yellow arrows, lateral membrane- yellow open
307 arrowhead, 5B and 5C), indicating disruption in cell polarity. *P. aeruginosa* infection
308 did not affect the position of AJ(Fig. 5A; cyan arrows).

309 The absence of intestinal deformation in *cdc-42(RNAi)* animals prompted us to
310 investigate if CDC-42 might also regulate apico-lateral polarity following *P. aeruginosa*
311 exposure. To this end, we checked the localization of LET-413 in control (L4440) and
312 *cdc-42(RNAi)* worms. The enhanced apical localization of LET-413 in the intestines of
313 control (L4440) worms was significantly diminished in *cdc-42(RNAi)* animals following
314 *P. aeruginosa* exposure (Fig. 5D). Conversely, we did not detect any disturbance to
315 the apical localization of CDC-42 and ARP-2/3 in *let-413(RNAi)* intestines, in
316 agreement with previous reports indicating that LET-413 depletion has minimal effect
317 on epithelial polarity (Fig S5A) (Riga *et al*, 2021). Moreover, similar to control animals,
318 *P. aeruginosa* exposure of *let-413(RNAi)* worms resulted in apical surface deformation
319 as well as elevated cytoplasmic levels of CDC-42 (S5A and S5B). Taken together,
320 these results suggest that upon exposure to *P. aeruginosa,* the apical surface *C.*
321 *elegans* intestine acquires basolateral characteristics in a CDC-42-dependent
322 mechanism.

323

324 **PI3K-AKT signalling is required for CDC-42 mis-localization and intestinal**
325 **deformation**

326 Disruption of the PI3K-AKT pathway impedes *P. aeruginosa* infection in MDCK cells
327 (Kierbel *et al*, 2005). Similarly, long-lived *C. elegans* mutants such as *akt-1*, *akt-2* and
328 *age-1*/PI3K exhibit resistance to *P. aeruginosa* (Evans *et al*, 2008; Garsin *et al*, 2003)
329 suggesting a conserved host response to *P. aeruginosa* infection between mammalian
330 epithelium and *C. elegans* enterocytes. To examine the conservation in cellular
331 response to *P. aeruginosa* between mammals and *C. elegans*, we diminished PI3K-
332 AKT signalling by a simultaneous depletion of AKT-1 and AKT-2 using RNAi and
333 checked the intestinal localization of LET-413, CDC-42 and ARX-2. Depletion of AKT-
334 1/AKT-2, like in *cdc-42(RNAi)* worms, prevented the apical localization of LET-413

following *P. aeruginosa* infection (Fig. 5D). Evidence for crosstalk between CDC-42 dependent actin assembly and PI3K-AKT in mammalian cells prompted us to measure CDC-42 and ARX-2 levels in the intestines of *akt-1(RNAi)+akt-2(RNAi)* and *age-1(RNAi)* animals following *P. aeruginosa* exposure (McCormick *et al*, 2019; Yang *et al*, 2012). Intestinal epithelium of animals depleted of AKT or AGE-1 displayed diminished apical and cytosolic ARX-2 localization compared to control animals (Fig. 5E, S5D - S5G), and also did not display apical deformation following *P. aeruginosa* exposure (Fig. 5F). Our results, taken together with earlier studies on MDCK cells (Kierbel *et al*, 2007) suggests that PI3K dependent apical enrichment of PI(3,4,5)P_3 following exposure to *P. aeruginosa*, disrupts apical membrane polarity and de-localizes ARP-2/3 dependent actin assembly from the apical surface resulting in intestinal deformation. These findings re-enforces the importance of polarity disruption as a key event following *P. aeruginosa* infection and prior to intestinal deformation.

Extracellular localization of *Pseudomonas* is sufficient to induce intestinal deformation

Pseudomonas aeruginosa functions both as an extracellular and intracellular pathogen infecting a wide range of hosts (Resko *et al*, 2024). Transient activation of PI3K pathway resulting in apical membrane acquiring basolateral characteristics was resulted in internalization of *P. aeruginosa* by MDCK cells (Kierbel *et al*, 2005). Electron microscopy studies of *P. aeruginosa* -infected *C. elegans* intestine have also reported *Pseudomonas* invasion into enterocytes (Irazoqui *et al*, 2010; Xue *et al*, 2024). To determine whether intestinal deformation in *C. elegans* results from *P. aeruginosa* breaching the epithelial barrier, we performed live confocal imaging of infection using GFP-expressing *E. coli* or *P. aeruginosa*. Unlike *E. coli* (OP50-GFP), which were in very few numbers even after two days of exposure, *P. aeruginosa* (PA14-GFP) cells formed visible aggregates throughout the intestinal lumen as early as one-day post infection (Fig. 6A). Interestingly, apical surfaces adjacent to these aggregates displayed mild contortions, which progressed into pronounced deformation by day 2 (Fig. 6A; red filled triangles in bottom row-PA14). Orthogonal reconstruction (YZ plane) of confocal (XY) planes revealed that PA14-GFP localization remained restricted to the lumen with no detectable signal in the cytoplasm of the

intestinal cells (Fig.6A; PA14 panel). These observations were confirmed using lattice light-sheet microscopy (Fig. 4C and Supplementary Movie S1). To test whether apical surface deformation is a general enterocyte response to any pathogen, we conducted parallel infection assays using *Salmonella enterica* serovar *typhimurium* (Stm), a Gram-negative bacterium known to modulate CDC-42 activity during mammalian infections (Bandyopadhyay *et al*, 2024) and cause lethality in *C. elegans (*Fig. S6A) (Aballay *et al*, 2000; Desai *et al*, 2019). Stm-GFP infection in worms expressing mCherry::ACT-5, resulted in efficient intestinal colonization by day 2 similar to *P. aeruginosa* (Fig. S6B). However, despite this robust lumen colonization, in contrast to *P. aeruginosa* , Stm-exposed intestines did not display any surface deformation (Fig. 6A; middle row, yellow open arrowheads). Taken together, these results indicate that the intestinal deformation is a pathogen-specific response by the *C. elegans* enterocyte to extracellular *Pseudomonas* infection.

Physical association between live *P .aeruginosa* and the intestinal surface is not essential for apical deformation

Given the key role for physical association with host cells in *P. aeruginosa* pathogenesis (via various adhesins, including flagella, type IV pili, type III secretion system (T3SS), and lectins (Bucior *et al*, 2012; Comolli *et al*, 1999; Thuenauer *et al*, 2022), we asked whether a direct attachment of *P. aeruginosa* to the apical membrane of *C. elegans* intestine was necessary to trigger tissue deformation. First, we tested if exposure to live microbes is essential for inducing deformation of apical surface, by exposing animals to heat-killed *E. coli* or *P. aeruginosa* instead of live bacteria. Since worms displayed no noticeable defects in growth, maturation or egg laying, we concluded that heat-killed bacteria as food source was not nutritionally limiting. However, unlike live *P. aeruginosa*, heat-killed *P. aeruginosa* failed to induce intestinal deformation (Fig. 6B; open red triangle). Our observation agrees with previous reports showing heat-killed *P. aeruginosa* does not elicit immune responses in *C.* elegans (Irazoqui *et al*, 2010). Since extracellular *P. aeruginosa* induces intestinal deformation, we hypothesized that secreted factors may mediate this effect. To test this, we exposed worms to cell-free filter-sterilized supernatant collected from *P. aeruginosa*

or *E. coli* cultures. Remarkably, a 12-hour exposure to *P. aeruginosa* supernatant alone was sufficient to trigger apical surface deformation in the *C. elegans* intestine (Fig. 6C).

The global response regulator, GacA governs the expression of numerous virulence factors secreted by *P. aeruginosa,* including toxins and components in biofilm regulation (Barta *et al*, 1992; Kitten *et al*, 1998; Parkins *et al*, 2001; Reimmann *et al*, 1997) and has also been implicated in inducing developmental defects and activating the unfolded protein response (UPR) in *C. elegans* intestinal epithelium (Pellegrino *et al*, 2014). To assess the role of GacA in apical surface deformation, we exposed mCherry::ACT-5-expressing worms to *E. coli*, *P. aeruginosa* or a *gacA* deletion mutant (PA14*ΔgacA*) strain. The intestines of worms exposed to PA14*ΔgacA* exhibited an intermediate level of intestinal deformation compared to those infected with wild-type PA14 (Fig. 6D and 6E). Importantly, a *gacA* deletion mutant (PA14*ΔgacA*) retains partial pathogenicity, causing ~50% lethality in infected worms (Fig. 6F) (Feinbaum *et al*, 2012; Tan *et al*, 1999b). These results suggest that while GacA partially contributes to *P. aeruginosa* pathogenesis in *C. elegans*, a GacA-independent mechanism also exists, through which the pathogen elicits tissue surface deformation. Taken together, these results support the view that while intestinal distension is a general tissue response to microbial colonization of the lumen, mechanical deformation of apical surface is a specific response to extracellular heat-labile component from *P. aeruginosa*.

DISCUSSION

Here we report that *P. aeruginosa* exposure induces two distinct morphological alterations in the *C. elegans* intestine; (a) lumenal distension, reflected by increased intestinal width, and (b) deformation of the apical surface, seen as wrinkling of the lumen. While lumen distension has been previously described as a general response to microbial colonisation, we show that apical surface deformation is specific to *P. aeruginosa* exposure.

427 *P. aeruginosa* infection in MDCK cells recruit PI3K to the attachment sites, causing
428 PIP_3 enrichment, apical mis-localization of basolateral proteins, and disruption of
429 epithelial polarity through perturbation of the Rho GTPases - RHO-1, RAC-1 and CDC-
430 42 (Aktories, 2011; Kazmierczak & Engel, 2002; Kierbel *et al*, 2007; Krall *et al*, 2000).
431 Consistent with this, we find that inhibition of either PI3K-AKT signalling or CDC-42-
432 dependent actin assembly diminished both intestinal deformation and pathogen-
433 induced lethality. *P. aeruginosa* infection also led to apical mis-localization of the
434 basolateral marker LET-413, indicating a loss of apical membrane identity, though no
435 apical markers were mis-localized basolaterally. The rescue observed in *cdc-42(RNAi)*
436 animals further implicated CDC-42 in pathogen-induced actin remodelling. However,
437 depletion of the downstream polarity factor, LET-413, failed to rescue deformation,
438 suggesting that CDC-42 contributes primarily via actin assembly rather than polarity
439 regulation. Supporting this, depletion of ACT-5 or disruption of ARP-2/3 phenocopied
440 *cdc-42(RNAi)*. In line with previous reports (Kierbel *et al*, 2005; Paradis & Ruvkun,
441 1998), we noted that attenuation of PI3K-AKT signalling rescued the intestinal
442 deformation by limiting ARP-2/3 mis-localization. Thus, manipulations that prevent
443 deformation were also found to extend survival, supporting a strong correlation
444 between intestinal cell surface mechanics and organism viability. These results
445 highlights the central role of CDC-42-ARP-2/3-mediated actin polymerization in *P.*
446 *aeruginosa*-induced deformation.

447 In uninfected animals, ARP-2/3, together with actin-binding proteins such as PLST-1
448 and FLN-2, forms evenly distributed apical clusters (Bidaud-Meynard *et al*, 2021).
449 ARP-2/3 polymerizes contiguous F-actin to support microvillar structures (Fig. 4A). *P.*
450 *aeruginosa* infection fragmented these clusters, disrupting local actin organization,
451 and destabilized the apical surface, promoting vesiculation of actin-rich membrane into
452 the lumen. Because apical actin structures in enterocytes show minimal mobility, their
453 disruption cannot be rapidly replenished, leading to progressive surface destabilization
454 (Bernadskaya *et al*, 2011; Bidaud-Meynard *et al*, 2021) (Fig. 6G). This is consistent
455 with electron micrographs showing actin protrusions in MDCK cells (Kierbel *et al*,
456 2005) and reports of microvillar loss and host debris accumulation in the *C. elegans*
457 lumen during *P. aeruginosa* infection (Irazoqui *et al*, 2010; Xue *et al*, 2024).
458 Intriguingly, depletion of ARX-2 or ACT-5 prevented vesicle release and surface

459 deformation, suggesting that a uniform depletion of ARP-2/3 or actin reduces the
460 availability of F-actin for vesiculation. A similar protective effect was observed in
461 MDCK cells, where Latrunculin A-mediated actin depolymerization attenuated *P.*
462 *aeruginosa* infection by up to 60-fold (Kazmierczak *et al*, 2004). CDC-42 upregulation
463 and activation have been reported in polarized MDCK cells (Kazmierczak *et al*, 2004).
464 While *P. aeruginosa* infection in *C. elegans* enterocytes led to cytoplasmic
465 accumulation of CDC-42, ARP-2/3 and actin, we suspect the accumulated CDC-42
466 and ARP-2/3 pools to be largely inactive, given that the cytoplasmic actin is primarily
467 G-actin. In mammals, RHO-mediated actin regulation and homeostasis are monitored
468 by pyrin- and NOD-dependent pathways, but no equivalent surveillance has been
469 reported in *C. elegans* (Mostowy & Shenoy, 2015). Although cytoplasmic actin
470 accumulation correlated with infection, it did not directly cause deformation. Whether
471 it may be sensed as a pattern of pathogenesis remains to be addressed. Moreover,
472 MAPK signalling remained intact in *cdc-42(RNAi)* animals following infection,
473 indicating that CDC-42 depletion does not impair microbial sensing.

474 *P. aeruginosa* is generally considered as an extracellular pathogen and its intracellular
475 lifestyle is usually associated with tissue injury. While *P. aeruginosa* has been shown
476 to infiltrate the cytoplasmic space in many host systems, we have not observed
477 epithelial breach in our experiments in the *C. elegans* intestine. The *C. elegans*
478 epithelium, similar to a fully confluent monolayer of polarized MDCK cells, is refractory
479 to intracellular *P. aeruginosa* infection. The surface deformation phenotype could,
480 however, be recapitulated by exposure to cell-free supernatant from *P. aeruginosa*
481 cultures but not by heat-killed bacteria suggested the role of a heat-labile factor. Given
482 the extracellular lifestyle of *P. aeruginosa* in polarized epithelia, extracellular
483 membrane vesicles (OMVs) rich in surface components, quorum-sensing molecules,
484 toxins and other virulence factors, are plausible mediators of deformation signal
485 (Bauman & Kuehn, 2009, 2006; Kuehn & Kesty, 2005; Mashburn & Whiteley, 2005).
486 Thus extracellular *P. aeruginosa* exploits PI3K-AKT activation to perturb ARP-2/3-
487 mediated actin organization, leading to the loss of apical polarity and cytoskeletal
488 integrity in *C. elegans* enterocytes. Our findings reveal an evolutionarily conserved
489 strategy by which *P. aeruginosa* subverts actin regulation during extracellular infection.
490 We speculate that pathogen-mediated disruption of polarity impairs apically directed

transport and secretion of antimicrobial peptides, and surface-binding lectins. An attenuated antimicrobial response could allow bacterial proliferation in the lumen and a rapid spreading of the bacteria in the population.

ACKNOWLEDGEMENTS

This work was supported by DBT-Wellcome India Alliance Fellowship (IA/I/18/1/503624) and ANRF Core research grant (CRG/2023/004638) to A.P, Department of Biotechnology Junior research Fellowship (DBT/2024-25/AshokaUni/2486) to T.S., and core funding support from the Trivedi School of Biosciences, Ashoka University. We acknowledge the infrastructure support from the Central Bio-imaging facility and Ashoka-Zeiss Core Imaging Facility at Ashoka University. We thank Ms. Megha Rai for help with vesicle size quantification, Ms. Shraddha Nirmal for technical assistance and Ms. Purna Pardeshi for some of the illustrations. We are grateful to the labs of Arnab Mukhopadhyay, Anindya Ghosh-Roy, Emily Troemel, Grégoire Michaux, Jogender Singh, Mike Boxem, Mahak Sharma and Varsha Singh, for sharing *C. elegans* and bacterial strains. Some strains were provided by the CGC, which is funded by NIH Office of Research Infrastructure Programs (P40OD010440). We tare grateful to Ishani Sharma, Saravanan Palani and Jogender Singh for their feedback on the manuscript.

AUTHOR CONTRIBUTIONS**:** D.A.N and A.P conceived the project. D.A.N, T.S and A.P designed the experiments. D.A.N and T.S performed experiments. D.A.N and T.S analysed the data with input from A.P. A.P wrote the manuscript with input from D.A.N and T.S.

Figure 1

Divyashree et. al (2025)

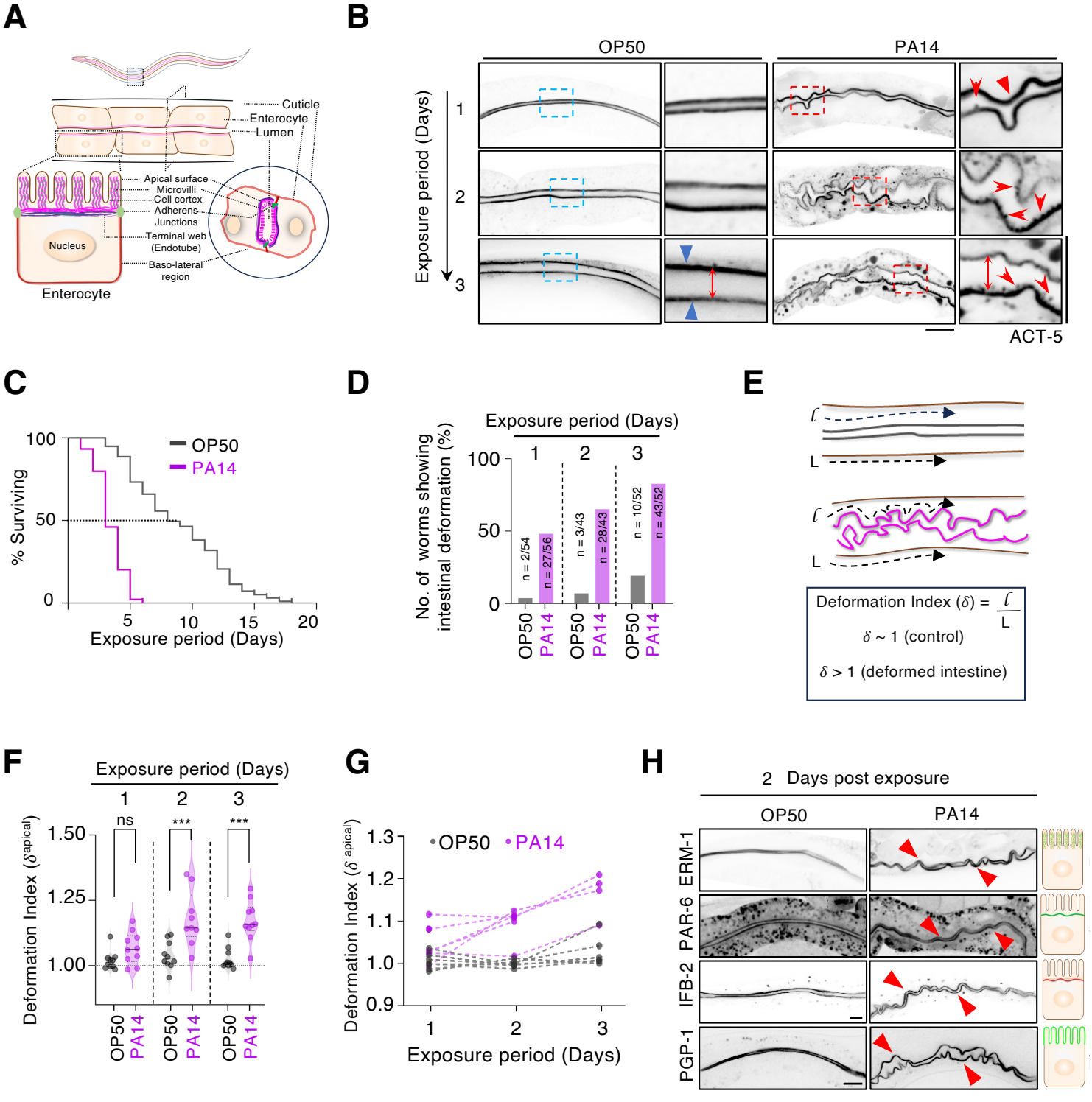

515 **Figure 1: *P. aeruginosa* infection deforms the apical surface of intestinal**
516 **epithelium in *C. elegans***

517 **(A)** Schematic illustration of *C. elegans* intestinal epithelium depicting different regions of the
518 enterocyte.

519 **(B)** Representative Kaplan-Meier survival plot of N2 worms infected with *P. aeruginosa* (PA14-
520 magenta) or *E. coli* (OP50-grey) at 25^0 C. (n = 100 worms, N=2)

521 **(C)** Medial confocal sections of *C. elegans* intestines expressing mCherry::ACT-5 localized to
522 apical surface. While lumen distension increases with age in animals exposed to with *P.*
523 *aeruginosa* or *E. coli* (red double headed arrows), intestinal surface deformation is seen only
524 upon exposure to with *P. aeruginosa* (red filled arrowheads), but not *E. coli* (blue ROI; blue
525 filled arrowheads). with *P. aeruginosa* infection also led to actin vesicles budding of apical
526 surface (Red ROI; red arrows).

527 **(D)** Bar graphs showing increased percentage of intestinal deformation with increase in the
528 duration of exposure to with *P. aeruginosa*.

529 **(E)** Schematic showing the estimation of deformation index (δ^{apical}) of apical surface

530 **(F)** Representative violin plot showing quantification of deformation index of apical surface
531 shown in Fig.1C. (N=3; n= 10 worms per treatment per set).

532 **(G)** Plot showing progressive deformation of apical surface of intestinal lumen from individual
533 worms measured over 3 days following *P. aeruginosa* or *E. coli* exposure. (n=5)

534 **(H)** Medial confocal images of *C. elegans* expressing fluorescently labelled apical markers
535 upon exposure to *P. aeruginosa* or *E. coli*. ERM-1::eGFP (apical regions containing microvilli),
536 PAR-6::mNeonGreen (apical PAR polarity complex), IFB-2::wScarlet (intermediate filaments),
537 PGP-1::GFP (apical plasma membrane).

538 Scale bar is 20 μm. P-values were calculated by Mann-Whitney U test. ****$p<0.0001$, ***p
539 <0.001, and * $p<0.05$
540

Figure 2

Divyashree et. al (2025)

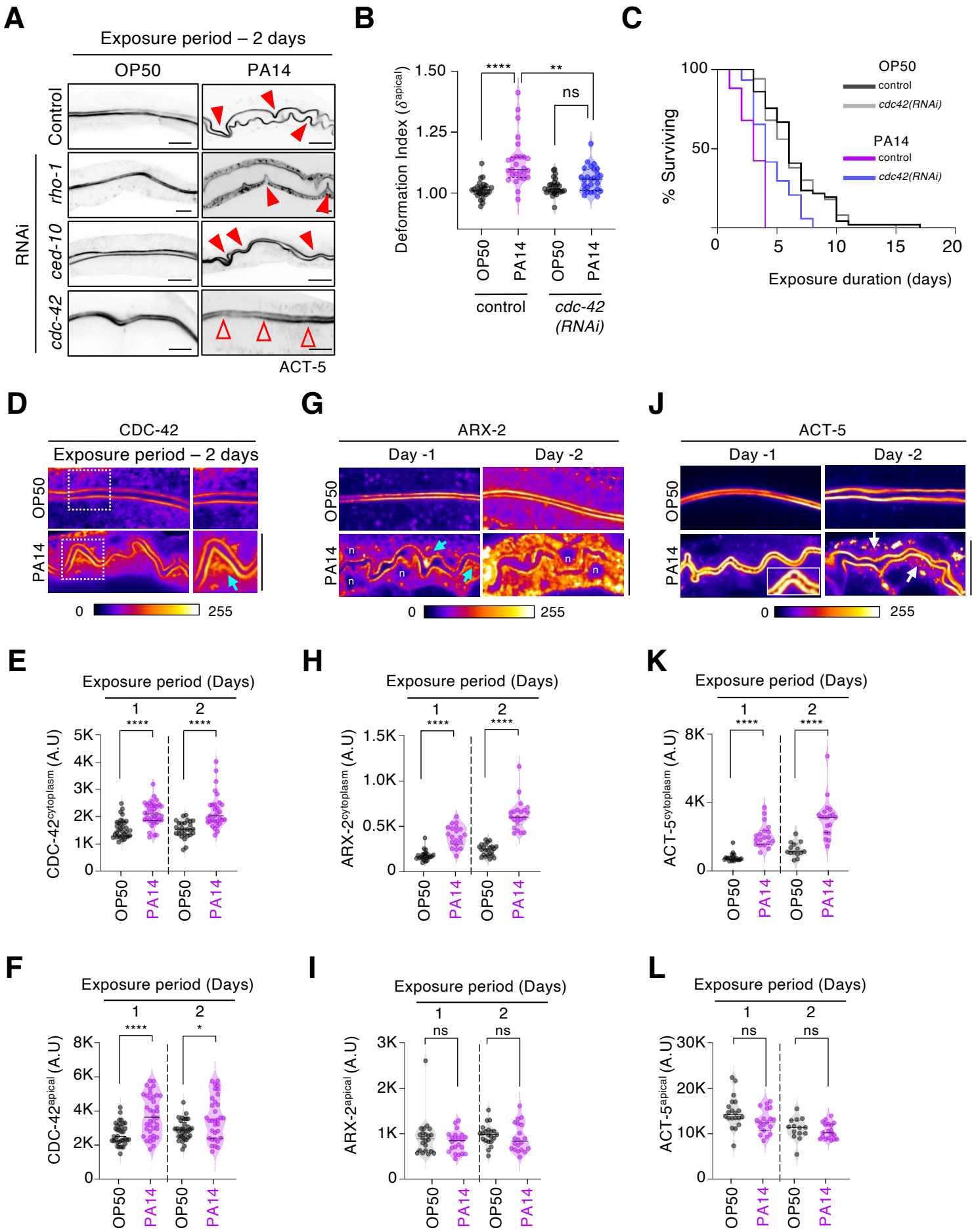

Figure 2: Exposure to *P. aeruginosa* results in cytoplasmic mis-localization of CDC-42, ARX-2 and ACT-5

(A) RNAi mediated depletion of *cdc-42*, but not *rho-1 or ced-10* rescues the *PA-14* induced intestinal deformation. Red filled arrowheads arrow heads show deformed regions of the lumen, while red open arrow heads denote the smooth intestinal lumen surface in *cdc-42(RNAi)* worms.

(B) Quantification showing reduced deformation index of intestines in *cdc-42(RNAi)* worms compared to L4440 (control) upon *P. aeruginosa* exposure for two days. Measurements are plotted as violin plot indicating median and interquartile of each data set. (N = 3; n=27))

(C) Representative Kaplan-Meier survival plot of *cdc-42(RNAi)* or L4440 (control) worms subjected to *P. aeruginosa* or *E. coli* infection. CDC-42 depletion partially rescues *P. aeruginosa* induced shortening of lifespan ($TD50^{cdc42(RNAi)}$ = 8 days, $TD50^{control}$ = 4 days) (N=2; n= 50 worms per set and per condition)

(D, G and J) Medial cross-sections of intestinal lumen of *C. elegans* expressing (D) CDC-42::GFP, (G) ARX-2::TagRFP, and (J) mCherry::ACT-5 following exposure to *E. coli* or *P. aeruginosa*. Images shown are pseudo-colored to highlight changes in the intensity. Warm colors represent higher intensity and lower intensity by the dimmer colors. Cyan arrows indicate the cytoplasmic enrichment of these proteins in animals infected with *P. aeruginosa*. Where visible, nuclei of the intestinal cells are marked with letter 'n'. Scale bar -20 μm.

(E and F) Violin plots showing cytoplasmic (E) and apical (F) intensities of CDC-42::GFP upon *P. aeruginosa* or *E. coli* infection. Measurements are mean ±95% C.I. Each dot represents one animal and the data shown is the cumulation of three independent experiments (N=3; n=33).

(H and I) Violin plots indicating cytoplasmic (E) and apical (F) intensities of ARX-2::TagRFP upon *P. aeruginosa* or *E. coli* infection. Measurements are mean ±95% C.I. Each dot represents individual worm (N=2; n≥21)

(K and L) Violin plots of cytoplasmic (E) and apical (F) intensity measurements of mCherry::ACT-5 upon *P. aeruginosa* or *E. coli* infection. Measurements are mean ±95% C.I. Each dot represents individual worm (N=2; n≥14)

Scale bar is 20 μm. P-values were calculated by Mann-Whitney U test. ****p<0.0001, ***p <0.001, **p <0.01and * p <0.05.

Figure 3

Divyashree et. al (2025)

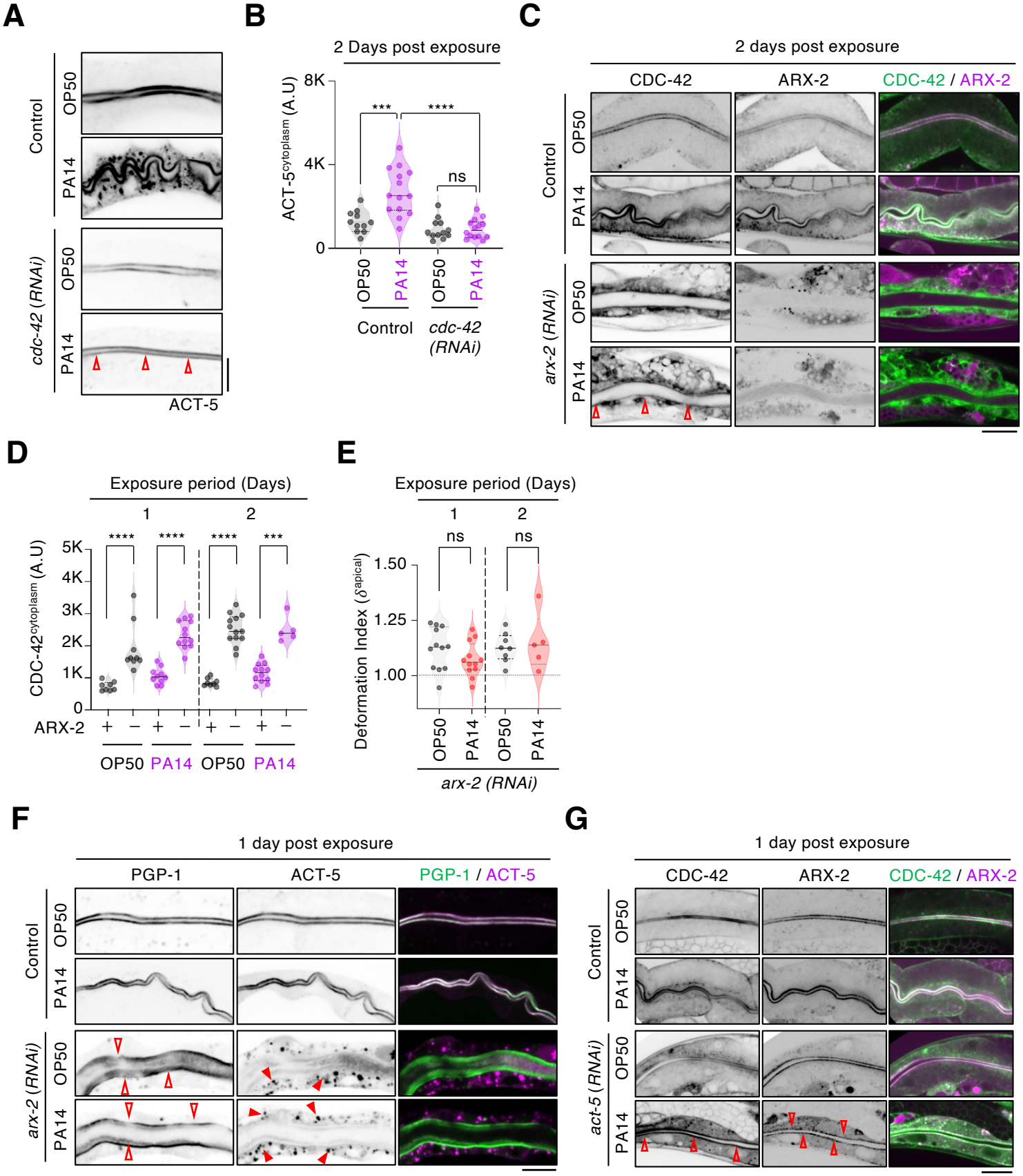

572 **Figure 3: Inhibition of ARP-2/3 dependent actin polymerization prevents *P.*
573 ***aeruginosa* -induced apical surface deformation**

574 **(A)** Intestinal lumen marked by mCherry::ACT-5 from control and *cdc-42(RNAi)* animals
575 exposed to *P. aeruginosa* or *E. coli*. Red arrowheads indicate rescue of intestinal deformation
576 in *cdc-42(RNAi)* animals.

577 **(B)** Cytoplasmic ACT-5 intensity quantified from intestinal epithelium of control and
578 *cdc42(RNAi)* worms, day 2 post infection. Quantifications are mean ±95% C.I. (n ≤ 14).

579 **(C)** Confocal images of intestinal epithelium from control and *arx-2(RNAi)* animals co-
580 expressing CDC-42::GFP and ARX-2::tagRFP, and subjected to *E. coli* and *P. aeruginosa*
581 infection. All images are from 2- days post infection. Open red arrows indicate rescue of the
582 intestinal deformation.

583 **(D)** Quantification of cytoplasmic CDC-42::GFP in control and *arx-2(RNAi)* animals following
584 2-day exposure to *P. aeruginosa* or *E. coli*. The violin plot shows the distribution of data with
585 median and interquartile for each data set. p-values n≥8 for all the sets. expect n= 5 for PA14
586 *arx-2 (RNAi)*.

587 **(E)** Violin plot showing apical deformation index quantification for *arx-2(RNAi)* animals
588 exposed to *E. coli* or *P. aeruginosa*. Plot shows the median and interquartile of each data set.
589 (n ≤ 11).

590 **(F)** Medial plane image of intestinal lumen co-expressing PGP1::GFP and mCherry::ACT5
591 subjected to control (L4440) and *arx-2* RNAi followed by *E. coli* and *Pseudomonas* exposure.
592 All the images are from one day post *E. coli* and *Pseudomonas* exposure.

593 **(G)** Medial plane image of intestinal lumen co-expressing CDC42::GFP and ARX2::TagRFP
594 subjected to control (L4440, empty vector) and *act-5* RNAi followed by *E. coli* and
595 *Pseudomonas* exposure. All the images are from one day post *E. coli* and *Pseudomonas*
596 exposure. Open red arrow marks represent rescue of the intestinal deformation.

597 unless otherwise specified, Scale bar is 20 μm. P-values were calculated by Mann-Whitney U
598 test. ****p<0.0001, ***p <0.001, and * p <0.05.

599

600

Figure 4

Divyashree et. al (2025)

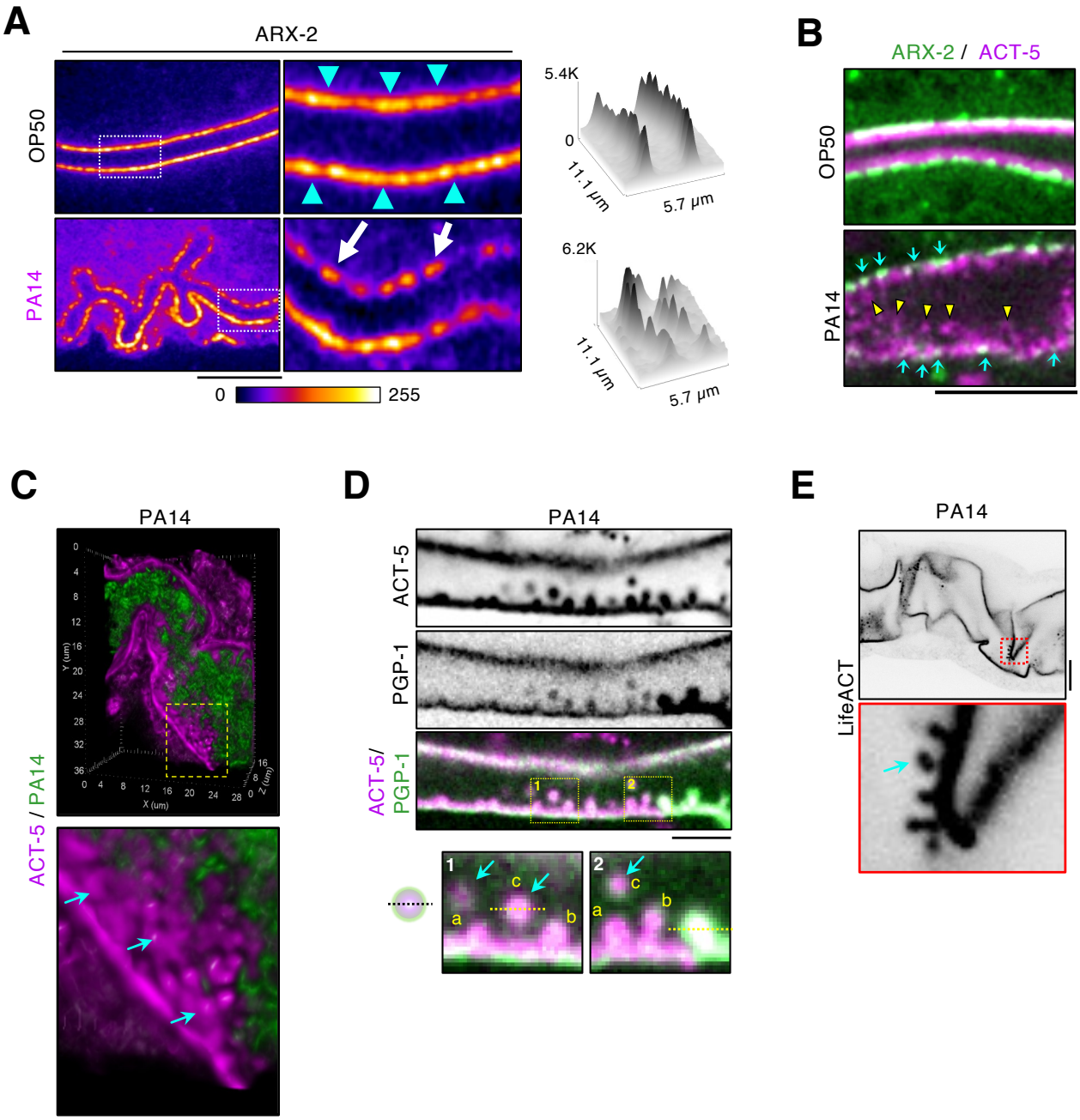

Figure 4: Fragmented ARP-2/3 disrupts actin assembly leading to extracellular vesicle release from apical surface

(A) Intensity visualization of medial confocal images of *C. elegans* intestines expressing ARX-2::TagRFP showing a fragmented distribution of ARX-2 (cyan arrows) on day-2 post *P. aeruginosa* exposure. ARX-2 shows a contiguous localization in worms exposed to *E. coli* (cyan arrowheads). Surface intensity of plots of enlarged ROIs highlights the fragmentation. Scale bar -10 μm.

(B) *C. elegans* co-expressing ARX-2::GFP and mCherry::ACT-5 showing actin structures (yellow arrowheads) permeating into the lumen from ARX-2-free regions (cyan arrows). Scale bar -10 μm.

(C) Lattice light sheet images acquired 2 days post exposure of PA14-GFP or OP50-GFP -fed *C. elegans* expressing intestinal mCherry::ACT5. Images were acquired in 13.3X objective and represented as maximum intensity projection in volume mode. Cyan arrows in enlarged ROI indicate the vesicles emerging from apical surface into the lumen.

(D) Membrane bound actin rich vesicles bud off from intestinal apical surface following 2-day *P. aeruginosa* exposure (cyan arrows in ROI). Enlarged ROI shows vesicles at various stages of budding – (a) initial bulging, (b) bud formation, and (c) released vesicle. An intensity linescan drawn across the extracellular vesicle indicates actin (magenta) surrounded by the apical plasma membrane marked by PGP-1::GFP (green). Scale bar - 5 μm.

(E) LifeACT::mRuby localizes to F-actin in the apical vesicles (cyan arrow) of *C. elegans* intestines exposed to *Pseudomonas*. Scale bar - 10 μm.

P-values were calculated by Mann -Whitney U test. ****$p<0.0001$, ***$p<0.001$, and * $p<0.05$.

Figure 5

Divyashree et. al (2025)

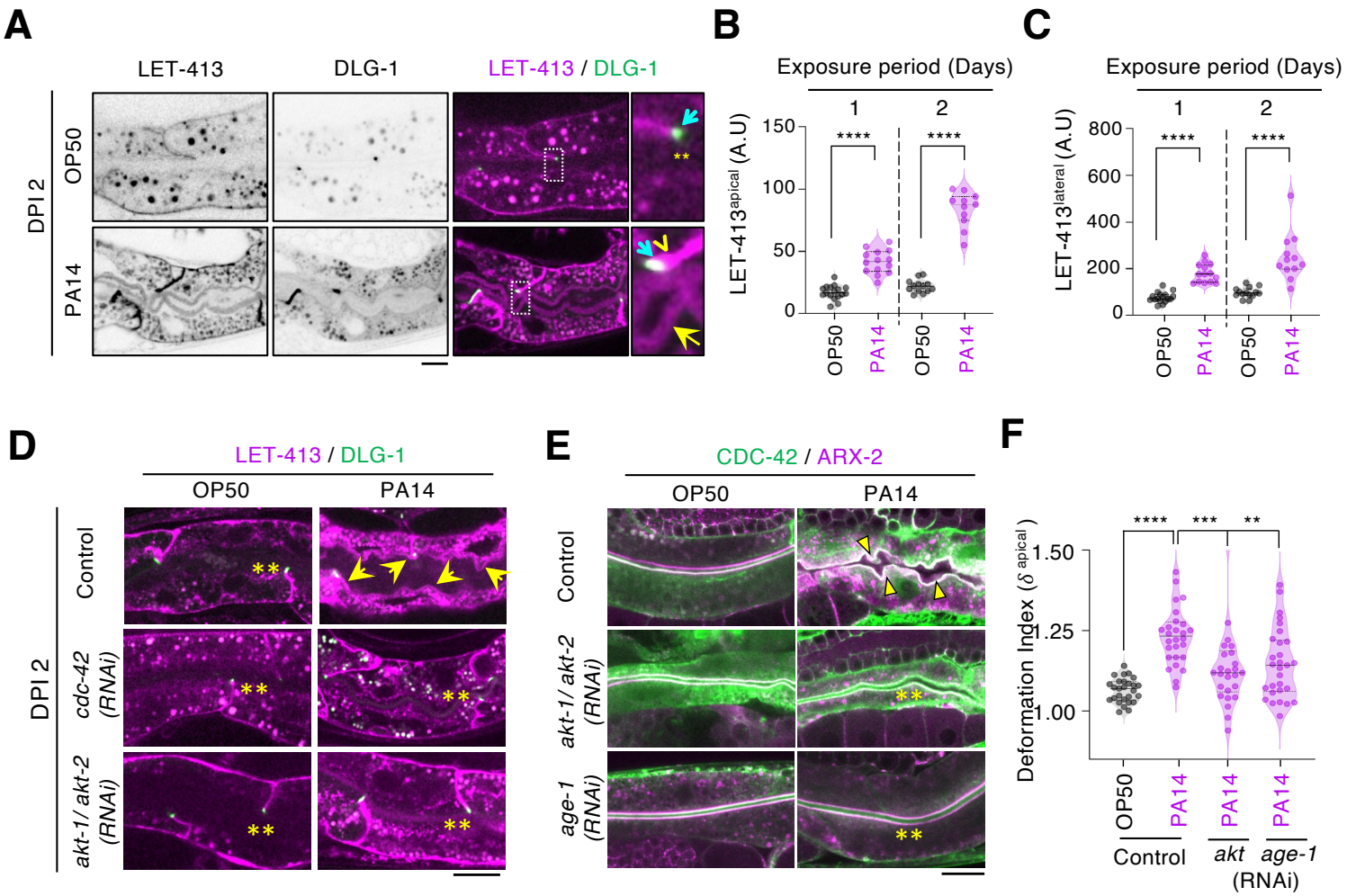

Figure 5 : *P. aeruginosa* induced polarity disruption is mediated via PI3K-AKT kinase pathway

(A) LET-413 shows enhanced accumulation in the apical (yellow arrow) and lateral (yellow arrowhead) surfaces *C. elegans* enterocytes upon *P. aeruginosa* infection. DLG-1 marks cell junctions (cyan arrows). Double asterisks shows absence of LET-413 at the apical surface in intestines of *C. elegans* exposed to *E. coli*.

(B and C) Quantification of (B) apical, and (C) lateral LET413 levels in enterocytes of worms following *E. coli* (OP50) or *P. aeruginosa* (PA14) infection. Each data point represents individual worm. Measurements are plotted as violin plot indicating median and interquartile of each data set. (n=12).

(D) Depletion of AKT-1 and AKT-2, or CDC-42 rescues *P. aeruginosa* induced loss of polarity. In contrast to control (L4440; yellow asterisks), apical recruitment of LET-413 in response to *P. aeruginosa* infection is absent in *akt-1/akt-2(RNAi)* and *cdc-42(RNAi)* (yellow asterisks).

(E) Disruption of PI3K-AKT pathway abrogates *P. aeruginosa* induced mis-localization of CDC-42, ARX-2 and actin. Medial confocal plane of intestinal lumen co-expressing CDC-42::GFP and ARX-2::TagRFP subjected to *akt-1/akt-2 and age-1* RNAi followed by *E. coli* and *Pseudomonas* exposure for two days. Closed yellow arrow indicate intestinal deformation. Yellow asterisks denote rescue of deformation.

(F) Violin plot showing apical deformation index(δ^{apical}) quantification for *akt-1/akt2* and *age-1(RNAi)* animals exposed to *E. coli* or *P. aeruginosa* for two days. Plot shows the median and interquartile of each data set (N =2, n≥22).

Scale bar in 20 μm. P-values were calculated by Mann -Whitney U test. ****p<0.0001, ***p <0.001, and **p <0.01

Figure 6

Divyashree et. al (2025)

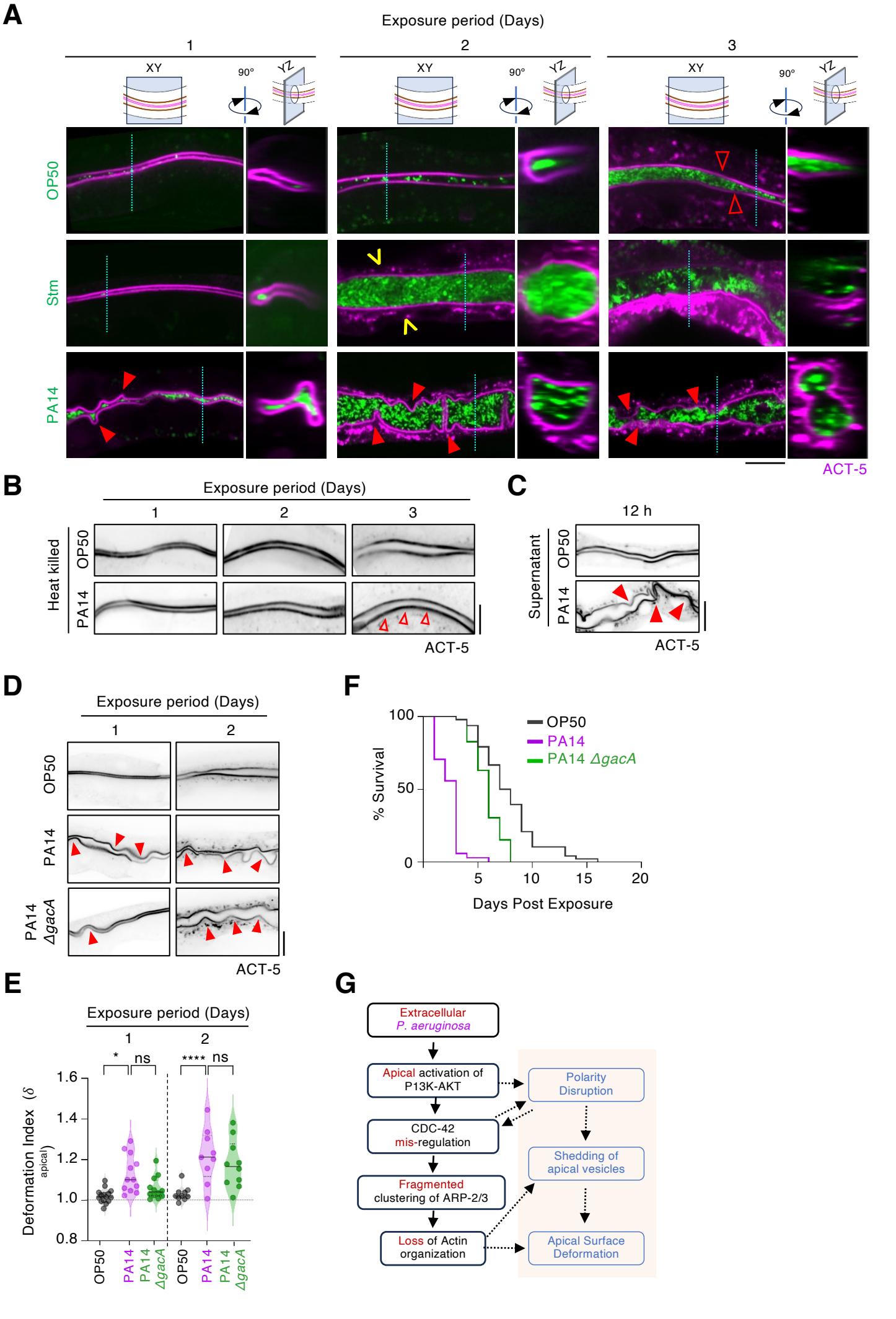

Figure 6: Extracellular *P. aeruginosa* can induce intestinal deformation in *C. elegans*

(A) Confocal medial images of intestinal epithelium from *C. elegans* expressing ACT-::mCherry and exposed to GFP expressing *E. coli* (top panel), *S. typhymurium* (middle panel) and *P. aeruginosa* (bottom panel) for 3-days post infection. Dashed lines indicate cross-sectional plane whose orthogonal view is presented adjacent to the image. Red hollow (*E. coli*) and yellow (*S. typhimurium)* arrowheads indicate intestinal distension (bloating), but smooth lumen surface. Red filled arrowheads indicate the deformation of the intestine in worms infected with *P. aeruginosa*.

(B) Medial confocal images of intestines from *C. elegans* expressing mCherry::ACT-5 animals grown on heat killed *E. coli* (top panel) and *P. aeruginosa* (bottom panel). Hollow red arrow indicates the absence of intestinal deformation upon exposure to heat killed *P. aeruginosa*.

(C) Medial confocal section of intestinal epithelium expressing mCherry::ACT5 exposed to 12 h of bacterial supernatant as indicated. Closed red arrows indicates intestinal deformation.

(D) Medial confocal images of intestines from *C.* elegans expressing mCherry::ACT-5 exposed to *E. coli*(OP50) (top panel), *P. aeruginosa* (PA14) (middle panel) and *P. aeruginosa* (PA14ΔgacA) (bottom panel). Filled red arrows indicates intestinal deformation.

(E) Quantification of deformation index (δ^{apical}) of the apical intestinal surface in C. elegans expressing intestinal mCherry::ACT-5 exposed to *E. coli*(OP50) ,*P. aeruginosa* (PA14) and *P. aeruginosa.* Each data point represents individual animal and measurements are plotted as violin plot indicating median and interquartile of each data set. (n =10)

(F) Kaplan- Meier survival plot of worms described in Fig. 6A upon exposure to *E. coli*(OP50), *P. aeruginosa* (PA14) and *GacA* deleted *P. aeruginosa* (PA14*Δgac*A) . Worms were grown on *E. coli* till L4 stage and transferred on to the respective infection plates. (n = 50 worms, N=2)

(G) Schematic of the proposed mechanism for *P. aeruginosa* induced intestinal apical surface deformation in *C. elegans.*

Scale bar in 20 μm. P-values were calculated by Mann -Whitney U test. ****$p<0.0001$, ***$p<0.001$, and * $p<0.05$

Graphical Abstract

Divyashree et. al (2025)

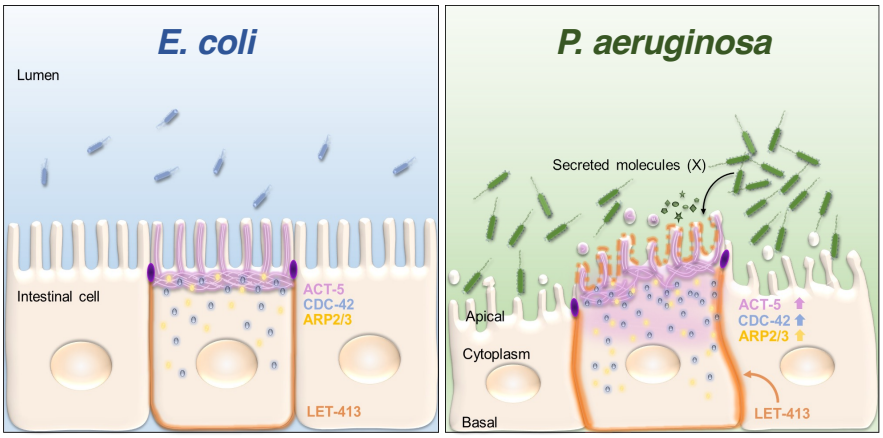

References:

Aballay A, Yorgey P & Ausubel FM (2000) Salmonella typhimurium proliferates and establishes a persistent infection in the intestine of Caenorhabditis elegans. *Curr Biol* 10: 1539–1542

Aktories K (2011) Bacterial protein toxins that modify host regulatory GTPases. *Nat Rev Microbiol* 9: 487–498

Ann Mack N & Georgiou M (2014) The interdependence of the Rho GTPases and apicobasal cell polarity. *Small GTPases* 5: 37–41

Armenti ST & Nance J (2012) Adherens junctions in C. elegans embryonic morphogenesis. *Subcell Biochem* 60: 279–299

Balla KM & Troemel ER (2013) Caenorhabditis elegans as a model for intracellular pathogen infection. *Cell Microbiol* 15: 1313–1322

Bandyopadhyay S, Zhang X, Ascura A, Edelblum KL, Bonder EM & Gao N (2024) Salmonella engages CDC42 effector protein 1 for intracellular invasion. *J Cell Physiol* 239

Barta TM, Kinscherf TG & Willis DK (1992) Regulation of tabtoxin production by the lemA gene in Pseudomonas syringae. *J Bacteriol* 174: 3021–3029

Bastounis EE, Radhakrishnan P, Prinz CK & Theriot JA (2022) Mechanical Forces Govern Interactions of Host Cells with Intracellular Bacterial Pathogens. *Microbiol Mol Biol Rev* 86: e00094-20

Bauman SJ & Kuehn MJ (2006) Purification of outer membrane vesicles from Pseudomonas aeruginosa and their activation of an IL-8 response. *Microbes Infect* 8: 2400–2408

Bauman SJ & Kuehn MJ (2009) Pseudomonas aeruginosa vesicles associate with and are internalized by human lung epithelial cells. *BMC Microbiol* 9: 26

Berg M, Stenuit B, Ho J, Wang A, Parke C, Knight M, Alvarez-Cohen L & Shapira M (2016) Assembly of the *Caenorhabditis elegans* gut microbiota from diverse soil microbial environments. *ISME J* 10: 1998–2009

Bernadskaya YY, Patel FB, Hsu HT & Soto MC (2011) Arp2/3 promotes junction formation and maintenance in the Caenorhabditis elegans intestine by regulating membrane association of apical proteins. *Mol Biol Cell* 22: 2886–2899

Bidaud-Meynard A, Demouchy F, Nicolle O, Pacquelet A, Suman SK, Plancke CN, Robin FB & Michaux G (2021) High-resolution dynamic mapping of the *C. elegans* intestinal brush border. *Development* 148

Bollen DP, Reddy KC, Lascarez-Lagunas LI, Kim DH & Colaiácovo MP (2024) Germline mitotic quiescence and cell death are induced in *Caenorhabditis elegans* by exposure to pathogenic *Pseudomonas aeruginosa*. *GENETICS* 226: iyad197

Bossinger O, Fukushige T, Claeys M, Borgonie G & McGhee JD (2004) The apical disposition of the Caenorhabditis elegans intestinal terminal web is maintained by LET-413. *Dev Biol* 268: 448–456

Bucior I, Pielage JF & Engel JN (2012) Pseudomonas aeruginosa Pili and Flagella Mediate Distinct Binding and Signaling Events at the Apical and Basolateral Surface of Airway Epithelium. *PLoS Pathog* 8: e1002616

Cohen LB & Troemel ER (2015) Microbial pathogenesis and host defense in the nematode C. elegans. *Curr Opin Microbiol* 23: 94–101

Colonne PM, Winchell CG & Voth DE (2016) Hijacking Host Cell Highways: Manipulation of the Host Actin Cytoskeleton by Obligate Intracellular Bacterial Pathogens. *Front Cell Infect Microbiol* 6

Comolli JC, Waite LL, Mostov KE & Engel JN (1999) Pili Binding to Asialo-GM1 on Epithelial Cells Can Mediate Cytotoxicity or Bacterial Internalization by *Pseudomonas aeruginosa*. *Infect Immun* 67: 3207–3214

Cowell BA, Evans DJ & Fleiszig SMJ (2005) Actin cytoskeleton disruption by ExoY and its effects on *Pseudomonas aeruginosa* invasion. *FEMS Microbiol Lett* 250: 71–76

Desai SK, Padmanabhan A, Harshe S, Zaidel-Bar R & Kenney LJ (2019) Salmonella biofilms program innate immunity for persistence in Caenorhabditis elegans. *Proc Natl Acad Sci U S A* 116: 12462–12467

Dimov I & Maduro MF (2019) The C. elegans intestine: organogenesis, digestion, and physiology. *Cell Tissue Res* 377: 383–396

Dunbar TL, Yan Z, Balla KM, Smelkinson MG & Troemel ER (2012) C. elegans detects pathogen-induced translational inhibition to activate immune signaling. *Cell Host Microbe* 11: 375–386

Egge N, Arneaud SLB, Wales P, Mihelakis M, McClendon J, Fonseca RS, Savelle C, Gonzalez I, Ghorashi A, Yadavalli S, *et al* (2019) Age-Onset Phosphorylation of a Minor Actin Variant Promotes Intestinal Barrier Dysfunction. *Dev Cell* 51: 587-601.e7

Estes KA, Dunbar TL, Powell JR, Ausubel FM & Troemel ER (2010) bZIP transcription factor zip-2 mediates an early response to Pseudomonas aeruginosa infection in Caenorhabditis elegans. *Proc Natl Acad Sci U S A* 107: 2153–2158

Evans EA, Chen WC & Tan M (2008) The DAF-2 insulin-like signaling pathway independently regulates aging and immunity in *C. elegans*. *Aging Cell* 7: 879–893

Ewbank J (2006) Signaling in the immune response. *WormBook*

Feinbaum RL, Urbach JM, Liberati NT, Djonovic S, Adonizio A, Carvunis A-R & Ausubel FM (2012) Genome-Wide Identification of Pseudomonas aeruginosa Virulence-Related Genes Using a Caenorhabditis elegans Infection Model. *PLoS Pathog* 8: e1002813

Filipowicz A, Lalsiamthara J & Aballay A (2021) TRPM channels mediate learned pathogen avoidance following intestinal distention. *eLife* 10: e65935

Fleiszig SM, Evans DJ, Do N, Vallas V, Shin S & Mostov KE (1997) Epithelial cell polarity affects susceptibility to Pseudomonas aeruginosa invasion and cytotoxicity. *Infect Immun* 65: 2861–2867

Garsin DA, Villanueva JM, Begun J, Kim DH, Sifri CD, Calderwood SB, Ruvkun G & Ausubel FM (2003) Long-Lived *C. elegans daf-2* Mutants Are Resistant to Bacterial Pathogens. *Science* 300: 1921–1921

Geisler F, Coch RA, Richardson C, Goldberg M, Bevilacqua C, Prevedel R & Leube RE (2020) Intestinal intermediate filament polypeptides in C. elegans: Common and isotype-specific contributions to intestinal ultrastructure and function. *Sci Rep* 10: 3142

Göbel V, Barrett PL, Hall DH & Fleming JT (2004) Lumen morphogenesis in C. elegans requires the membrane-cytoskeleton linker erm-1. *Dev Cell* 6: 865–873

Gravato-Nobre MJ, Nicholas HR, Nijland R, O'Rourke D, Whittington DE, Yook KJ & Hodgkin J (2005) Multiple genes affect sensitivity of Caenorhabditis elegans to the bacterial pathogen Microbacterium nematophilum. *Genetics* 171: 1033–1045

Irazoqui JE, Troemel ER, Feinbaum RL, Luhachack LG, Cezairliyan BO & Ausubel FM (2010) Distinct Pathogenesis and Host Responses during Infection of C. elegans by P. aeruginosa and S. aureus. *PLoS Pathog* 6: e1000982

Jaffe AB & Hall A (2005) Rho GTPases: Biochemistry and biology. *Annu Rev Cell Dev Biol* 21: 247–269

Kazmierczak BI & Engel JN (2002) *Pseudomonas aeruginosa* ExoT Acts In Vivo as a GTPase-Activating Protein for RhoA, Rac1, and Cdc42. *Infect Immun* 70: 2198–2205

Kazmierczak BI, Mostov K & Engel JN (2004) Epithelial Cell Polarity Alters Rho-GTPase Responses to *Pseudomonas aeruginosa*. *Mol Biol Cell* 15: 411–419

Kierbel A, Gassama-Diagne A, Mostov K & Engel JN (2005) The Phosphoinositol-3-Kinase–Protein Kinase B/Akt Pathway Is Critical for *Pseudomonas aeruginosa* Strain PAK Internalization. *Mol Biol Cell* 16: 2577–2585

Kierbel A, Gassama-Diagne A, Rocha C, Radoshevich L, Olson J, Mostov K & Engel J (2007) *Pseudomonas aeruginosa* exploits a PIP3-dependent pathway to transform apical into basolateral membrane. *J Cell Biol* 177: 21–27

Kitten T, Kinscherf TG, McEvoy JL & Willis DK (1998) A newly identified regulator is required for virulence and toxin production in Pseudomonas syringae. *Mol Microbiol* 28: 917–929

Krall R, Schmidt G, Aktories K & Barbieri JT (2000) Pseudomonas aeruginosa ExoT is a Rho GTPase-activating protein. *Infect Immun* 68: 6066–6068

Kuehn MJ & Kesty NC (2005) Bacterial outer membrane vesicles and the host–pathogen interaction. *Genes Dev* 19: 2645–2655

Kumar S, Egan BM, Kocsisova Z, Schneider DL, Murphy JT, Diwan A & Kornfeld K (2019) Lifespan Extension in C. elegans Caused by Bacterial Colonization of the Intestine and Subsequent Activation of an Innate Immune Response. *Dev Cell* 49: 100-117.e6

Kuss-Duerkop SK & Keestra-Gounder AM (2020) NOD1 and NOD2 Activation by Diverse Stimuli: a Possible Role for Sensing Pathogen-Induced Endoplasmic Reticulum Stress. *Infect Immun* 88: e00898-19

Legouis R, Gansmuller A, Sookhareea S, Bosher JM, Baillie DL & Labouesse M (2000) LET-413 is a basolateral protein required for the assembly of adherens junctions in Caenorhabditis elegans. *Nat Cell Biol* 2: 415–422

Lei M, Tan Y, Tu H & Tan W (2024) Neuronal basis and diverse mechanisms of pathogen avoidance in Caenorhabditis elegans. *Front Immunol* 15: 1353747

Ma L, Rohatgi R & Kirschner MW (1998) The Arp2/3 complex mediates actin polymerization induced by the small GTP-binding protein Cdc42. *Proc Natl Acad Sci U S A* 95: 15362–15367

MacQueen AJ, Baggett JJ, Perumov N, Bauer RA, Januszewski T, Schriefer L & Waddle JA (2005a) ACT-5 Is an Essential *Caenorhabditis elegans* Actin Required for Intestinal Microvilli Formation. *Mol Biol Cell* 16: 3247–3259

MacQueen AJ, Baggett JJ, Perumov N, Bauer RA, Januszewski T, Schriefer L & Waddle JA (2005b) ACT-5 Is an Essential *Caenorhabditis elegans* Actin Required for Intestinal Microvilli Formation. *Mol Biol Cell* 16: 3247–3259

Mahajan-Miklos S, Tan M-W, Rahme LG & Ausubel FM (1999) Molecular Mechanisms of Bacterial Virulence Elucidated Using a Pseudomonas aeruginosa–Caenorhabditis elegans Pathogenesis Model. *Cell* 96: 47–56

Martin-Belmonte F, Gassama A, Datta A, Yu W, Rescher U, Gerke V & Mostov K (2007) PTEN-Mediated Apical Segregation of Phosphoinositides Controls Epithelial Morphogenesis through Cdc42. *Cell* 128: 383–397

Mashburn LM & Whiteley M (2005) Membrane vesicles traffic signals and facilitate group activities in a prokaryote. *Nature* 437: 422–425

McCormick B, Chu JY & Vermeren S (2019) Cross-talk between Rho GTPases and PI3K in the neutrophil. *Small GTPases* 10: 187–195

McEwan DL, Kirienko NV & Ausubel FM (2012) Host translational inhibition by Pseudomonas aeruginosa exotoxin A triggers an immune response in Caenorhabditis elegans. *Cell Host Microbe* 11: 364–374

McGhee J (2007) The C. elegans intestine. *WormBook*

McMahon L, Legouis R, Vonesch JL & Labouesse M (2001) Assembly of C. elegans apical junctions involves positioning and compaction by LET-413 and protein aggregation by the MAGUK protein DLG-1. *J Cell Sci* 114: 2265–2277

Melo JA & Ruvkun G (2012) Inactivation of conserved C. elegans genes engages pathogen- and xenobiotic-associated defenses. *Cell* 149: 452–466

Mostowy S & Shenoy AR (2015) The cytoskeleton in cell-autonomous immunity: structural determinants of host defence. *Nat Rev Immunol* 15: 559–573

Neukomm LJ, Zeng S, Frei AP, Huegli PA & Hengartner MO (2014) Small GTPase CDC-42 promotes apoptotic cell corpse clearance in response to PAT-2 and CED-1 in C. elegans. *Cell Death Differ* 21: 845–853

Paradis S & Ruvkun G (1998) *Caenorhabditis elegans* Akt/PKB transduces insulin receptor-like signals from AGE-1 PI3 kinase to the DAF-16 transcription factor. *Genes Dev* 12: 2488–2498

Parkins MD, Ceri H & Storey DG (2001) Pseudomonas aeruginosa GacA, a factor in multihost virulence, is also essential for biofilm formation. *Mol Microbiol* 40: 1215–1226

Pederson KJ, Vallis AJ, Aktories K, Frank DW & Barbieri JT (1999) The amino-terminal domain of *Pseudomonas aeruginosa* ExoS disrupts actin filaments via small-molecular-weight GTP-binding proteins. *Mol Microbiol* 32: 393–401

Pellegrino MW, Nargund AM, Kirienko NV, Gillis R, Fiorese CJ & Haynes CM (2014) Mitochondrial UPR-regulated innate immunity provides resistance to pathogen infection. *Nature* 516: 414–417

Pereira AG, Gracida X, Kagias K & Zhang Y (2020) *C. elegans* aversive olfactory learning generates diverse intergenerational effects. *J Neurogenet* 34: 378–388

Peterson ND, Icso JD, Salisbury JE, Rodríguez T, Thompson PR & Pukkila-Worley R (2022) Pathogen infection and cholesterol deficiency activate the C. elegans p38 immune pathway through a TIR-1/SARM1 phase transition. *eLife* 11: e74206

Peterson ND, Tse SY, Huang QJ, Wani KA, Schiffer CA & Pukkila-Worley R (2023) Non-canonical pattern recognition of a pathogen-derived metabolite by a nuclear hormone receptor identifies virulent bacteria in C. elegans. *Immunity* 56: 768-782.e9

Prakash D, Ms A, Radhika B, Venkatesan R, Chalasani SH & Singh V (2021) 1-Undecene from *Pseudomonas aeruginosa* is an olfactory signal for flight-or-fight response in *Caenorhabditis elegans*. *EMBO J* 40: e106938

Pukkila-Worley R & Ausubel FM (2012) Immune defense mechanisms in the Caenorhabditis elegans intestinal epithelium. *Curr Opin Immunol* 24: 3–9

Reimmann C, Beyeler M, Latifi A, Winteler H, Foglino M, Lazdunski A & Haas D (1997) The global activator GacA of Pseudomonas aeruginosa PAO positively controls the production of the autoinducer N-butyryl-homoserine lactone and the formation of the virulence factors pyocyanin, cyanide, and lipase. *Mol Microbiol* 24: 309–319

Resko ZJ, Suhi RF, Thota AV & Kroken AR (2024) Evidence for intracellular *Pseudomonas aeruginosa*. *J Bacteriol* 206

Riga A, Cravo J, Schmidt R, Pires HR, Castiglioni VG, Van Den Heuvel S & Boxem M (2021) Caenorhabditis elegans LET-413 Scribble is essential in the epidermis for growth, viability, and directional outgrowth of epithelial seam cells. *PLOS Genet* 17: e1009856

Ruch TR & Engel JN (2017) Targeting the Mucosal Barrier: How Pathogens Modulate the Cellular Polarity Network. *Cold Spring Harb Perspect Biol* 9: a027953

Schulenburg H & Félix M-A (2017) The Natural Biotic Environment of*Caenorhabditis elegans*. *Genetics* 206: 55–86

Sepers JJ, Ramalho JJ, Kroll JR, Schmidt R & Boxem M (2022) ERM-1 Phosphorylation and NRFL-1 Redundantly Control Lumen Formation in the C. elegans Intestine. *Front Cell Dev Biol* 10

Shafaq-Zadah M, Brocard L, Solari F & Michaux G (2012) AP-1 is required for the maintenance of apico-basal polarity in the*C. elegans*intestine. *Development* 139: 2061–2070

Singh J & Aballay A (2019a) Microbial Colonization Activates an Immune Fight-and-Flight Response via Neuroendocrine Signaling. *Dev Cell* 49: 89-99.e4

Singh J & Aballay A (2019b) Intestinal infection regulates behavior and learning via neuroendocrine signaling. *eLife* 8: e50033

Stiernagle T (2006) Maintenance of C. elegans. *WormBook*

Stuart LM, Paquette N & Boyer L (2013) Effector-triggered versus pattern-triggered immunity: how animals sense pathogens. *Nat Rev Immunol* 13: 199–206

Stutz K, Kaech A, Aebi M, Künzler M & Hengartner MO (2015) Disruption of the C. elegans intestinal brush border by the fungal lectin CCL2 phenocopies dietary lectin toxicity in mammals. *PLoS ONE* 10: 1–23

895 Sun J & Barbieri JT (2004) ExoS Rho GTPase-activating Protein Activity Stimulates
896 Reorganization of the Actin Cytoskeleton through Rho GTPase Guanine
897 Nucleotide Disassociation Inhibitor. *J Biol Chem* 279: 42936–42944

898 Szumowski SC, Estes KA, Popovich JJ, Botts MR, Sek G & Troemel ER (2016) Small
899 GTPases promote actin coat formation on microsporidian pathogens traversing
900 the apical membrane of*Caenorhabditis elegans*intestinal cells: Actin coats on
901 microsporidia-containing vesicles. *Cell Microbiol* 18: 30–45

902 Tan MW, Mahajan-Miklos S & Ausubel FM (1999a) Killing of Caenorhabditis elegans by
903 Pseudomonas aeruginosa used to model mammalian bacterial pathogenesis.
904 *Proc Natl Acad Sci U S A* 96: 715–720

905 Tan M-W, Rahme LG, Sternberg JA, Tompkins RG & Ausubel FM (1999b) *Pseudomonas*
906 *aeruginosa* killing of *Caenorhabditis elegans* used to identify *P. aeruginosa*
907 virulence factors. *Proc Natl Acad Sci* 96: 2408–2413

908 Thuenauer R, Kühn K, Guo Y, Kotsis F, Xu M, Trefzer A, Altmann S, Wehrum S,
909 Heshmatpour N, Faust B, *et al* (2022) The Lectin LecB Induces Patches with
910 Basolateral Characteristics at the Apical Membrane to Promote Pseudomonas
911 aeruginosa Host Cell Invasion. *mBio* 13: e00819-22

912 Tran CS, Eran Y, Ruch TR, Bryant DM, Datta A, Brakeman P, Kierbel A, Wittmann T,
913 Metzger RJ, Mostov KE, *et al* (2014) Host Cell Polarity Proteins Participate in
914 Innate Immunity to Pseudomonas aeruginosa Infection. *Cell Host Microbe* 15:
915 636–643

916 Tse-Kang S, Wani KA & Pukkila-Worley R (2025) Patterns of pathogenesis in innate
917 immunity: insights from C. elegans. *Nat Rev Immunol*

918 Vance RE, Isberg RR & Portnoy DA (2009) Patterns of Pathogenesis: Discrimination of
919 Pathogenic and Nonpathogenic Microbes by the Innate Immune System. *Cell*
920 *Host Microbe* 6: 10–21

921 Winter JF, Höpfner S, Korn K, Farnung BO, Bradshaw CR, Marsico G, Volkmer M,
922 Habermann B & Zerial M (2012) Caenorhabditis elegans screen reveals role of
923 PAR-5 in RAB-11-recycling endosome positioning and apicobasal cell polarity.
924 *Nat Cell Biol* 14: 666–676

925 Wu D, Chai Y, Zhu Z, Li W, Ou G & Li W (2017) CED-10-WASP-Arp2/3 signaling axis
926 regulates apoptotic cell corpse engulfment in C. elegans. *Dev Biol* 428: 215–223

927 Xue F, Ragno M, Blackburn SA, Fasseas M, Maitra S, Liang M, Rai S, Mastroianni G,
928 Tholozan F, Thompson R, *et al* (2024) New tools to monitor Pseudomonas
929 aeruginosa infection and biofilms in vivo in C. elegans. *Front Cell Infect Microbiol*
930 14

931 Yang HW, Shin M-G, Lee S, Kim J-R, Park WS, Cho K-H, Meyer T & Do Heo W (2012)
932 Cooperative Activation of PI3K by Ras and Rho Family Small GTPases. *Mol Cell*
933 47: 281–290

Zhang Y, Lu H & Bargmann CI (2005) Pathogenic bacteria induce aversive olfactory learning in Caenorhabditis elegans. *Nature* 438: 179–184